Eur Biophys J (2012) 41:695–704
DOI 10.1007/s00249-012-0846-0

ORIGINAL PAPER

EBSA
Biophysics in Europe

Inhibition of semen-derived enhancer of virus infection (SEVI) fibrillogenesis by zinc and copper

Sarah R. Sheftic · Jessica M. Snell · Suman Jha · Andrei T. Alexandrescu

Received: 4 June 2012 / Revised: 15 July 2012 / Accepted: 27 July 2012 / Published online: 21 August 2012

Abstract Semen-derived enhancer of virus infection (SEVI), a naturally occurring peptide fragment of prostatic acid phosphatase, enhances HIV infectivity by forming cationic amyloid fibrils that aid the fusion of negatively charged virion and target cell membranes. Cu(II) and Zn(II) inhibit fibrillization of SEVI in a kinetic assay using the fibril-specific dye ThT. TEM suggests that the metals do not affect fibril morphology. NMR shows that the metals bind to histidines 3 and 23 in the SEVI sequence. ITC experiments indicate that SEVI forms oligomeric complexes with the metals. Dissociation constants are micromolar for Cu(II) and millimolar for Zn(II). Because the Cu(II) and Zn(II) concentrations that inhibit fibrillization are comparable with those found in seminal fluid the metals may modulate SEVI fibrillization under physiological conditions.

Keywords Intrinsically unfolded peptide · Fibrillization inhibitor · Sexual transmission · Human immunodeficiency virus · Histidine ionization · Amyloidogenic protein

Abbreviations

DMSO	Dimethyl sulfoxide
EDTA	Ethylenediaminetetraacetic acid
ITC	Isothermal titration calorimetry
HIV	Human immunodeficiency virus
HSQC	Heteronuclear single-quantum coherence
NMR	Nuclear magnetic resonance
NOESY	Nuclear Overhauser enhancement spectroscopy
PBS	Phosphate-buffered saline
TBS	Tris-buffered saline
TEM	Transmission electron microscopy
ThT	Thioflavin T
TOCSY	Total correlation spectroscopy
SEVI	Semen-derived enhancer of virus infection—in this case, specifically the 248–286 fragment of human prostatic acid phosphatase: $PAP_{248–286}$

Introduction

Semen-derived enhancer of virus infection (SEVI) is a naturally occurring 39-residue (4.6-kDa) proteolytic fragment of human prostatic acidic phosphatase ($PAP_{248–286}$) that was discovered during screening of semen compounds for effects on HIV infectivity (Munch et al. 2007). The SEVI peptide is present at a concentration of ~35 μg/ml in semen, and can assemble into amyloid fibrils with a cross β-sheet structure at concentrations above 2 μg/ml (Munch et al. 2007). The fibrils attach to virions and facilitate their fusion to target cells, thereby increasing HIV infectivity up to 400,000-fold (Munch et al. 2007). As such, the SEVI peptide could be an important facilitator of HIV transmission.

The authors Sarah R. Sheftic and Jessica M. Snell contributed equally to this work.

Electronic supplementary material The online version of this article (doi:10.1007/s00249-012-0846-0) contains supplementary material, which is available to authorized users.

S. R. Sheftic · J. M. Snell · S. Jha · A. T. Alexandrescu (✉)
Department of Molecular and Cell Biology,
University of Connecticut, 91 N. Eagleville Rd.,
Storrs, CT 06269-3125, USA
e-mail: andrei@uconn.edu

The positively charged amyloid fibrils formed by SEVI are thought to promote viral fusion by reducing electrostatic repulsion between negatively charged virus and target cell membranes (Kim et al. (2010); Munch et al. 2007; Roan et al. 2009). The activity of SEVI seems to be general, in that it promotes cell-fusion of a variety of HIV variants (Munch et al. 2007) and human XMRV, a retrovirus which may be involved in prostate cancer (Hong et al. 2009). SEVI also boosts infectivity nonspecifically for a number of other retroviruses—a finding that may have applications to therapeutic gene transfer (Wurm et al. 2010). The generality of the charge-screening mechanism is further emphasized by the observation that designed peptides, with sequences unrelated to SEVI, retain the ability to enhance HIV infectivity as long as they assemble into fibrils with cationic surfaces (Easterhoff et al. 2011).

Semen contains a very complex mixture of compounds (Huang et al. 2000; Martellini et al. 2011; Munch et al. 2007; Owen and Katz 2005). It has been shown recently that anionic buffer molecules in human seminal plasma accelerate fibrillization (Olsen et al. 2012), whereas other components, for example proteases, inhibit fibrillization by degrading SEVI (Martellini et al. 2011). In this work, we focus on how SEVI fibrillization is affected by heavy metals, because these are found at large concentrations in seminal plasma and have been shown to modulate the fibrillization of other amyloidogenic proteins and peptides, including A-β (Tougu et al. 2011), amylin (Brender et al. 2010; Salamekh et al. 2011), α-synuclein (Santner and Uversky 2010), β-microglobulin (Morgan et al. 2001), insulin (Noormagi et al. 2010), and prion protein (Singh et al. 2010). We show that Cu^{2+} and Zn^{2+} inhibit fibrillization in a kinetic assay using the amyloid-specific fluorescent dye ThT, but that TEM shows the morphology of the resulting fibrils is unaffected. NMR used to map the binding sites of Cu^{2+} and Zn^{2+} to two histidines in the SEVI amino acid sequence. ITC was used to determine the stoichiometry and binding affinity of SEVI for the two metals.

Materials and methods

Materials

SEVI was purchased as a custom-synthesized peptide from Biopeptide (San Diego, CA, USA). The samples were 95 % pure by HPLC and had a peptide content of 70 %. Samples were received as lyophilized powders and resuspended in 100 % DMSO to make stock solutions of 100 mg/ml peptide. The stock solutions were kept at −80 °C when not in use. For experiments, SEVI stocks were diluted with the desired buffers to a final concentration of 4 % (*v*/*v*) DMSO. $CuCl_2$, $ZnCl_2$, $MgCl_2$, and $CaCl_2$ were from Sigma. EDTA was from Fisher. All buffers were prepared with Milli-Q water and filtered through a 0.22 μm Millipore filter before use. Buffers for monitoring fibril formation were also treated with Chelex-100 to remove trace metals, in accordance with the manufacturer's instructions (Bio-Rad, Hercules CA, USA).

Fibril formation kinetics

Fibril kinetic assays were conducted in white 96-well clear-bottom Corning Costar plates (Lowell, MA, USA) sealed with clear polyester tape to prevent evaporation. Unless otherwise specified, 200-μl samples were used with 2 mg/ml of SEVI in pH 7.4 PBS buffer (8 mM Na_2HPO_4, 1.8 mM KH_2PO_4, 2.7 mM KCl, and 140 mM NaCl). The SEVI concentration used for this work is lower than the 5–10 mg/ml typically used in previous studies (Hauber et al. 2009; Munch et al. 2007; Olsen et al. 2010; Roan et al. 2009). The peptide concentration was chosen as a compromise between peptide cost and the time required to complete fibrillization, because reproducibility worsens with increasing reaction times (Giehm and Otzen 2010). We examined a series of SEVI concentrations between 0.1 and 5 mg/ml and found that the ThT fluorescence plateaus for the fibrillization reactions scale nearly linearly, except at high peptide concentrations (Supplementary Fig. S1), at which nonspecific aggregation may start to compete with fibrillization (Noormagi et al. 2010).

A potential problem with the phosphate buffer used in this work is that it can cause precipitation of metals, and form complexes which reduce the free metal ion concentration (Aslamkhan et al. 2002; Collier 1979). The precipitating phosphate (PO_4^{3-}) ion forms with a pK_a of 12.6, so that at a physiological pH of 7.4 its concentration will be only 0.006 % of the total phosphate concentration, namely 0.6 μM for 10 mM phosphate buffer (Aslamkhan et al. 2002). Consistently, we saw no visible precipitation in the samples even at the highest metal concentrations, 1 mM, used in our PBS buffer. Because the metals can form soluble complexes with $H_2PO_4^-$ and HPO_4^{2-} ions, however, the effective free metal concentration in solution may be as much as a factor of ten lower than the total metal concentration (Collier 1979). As an alternative to phosphate, we conducted experiments in 20 mM Tris–150 mM NaCl (TBS) buffer at pH 7.4, and saw a dependence on $CuCl_2$ concentration similar to that observed in PBS. On the basis of the ThT fluorescence plateaus at the end of the reaction, however, the amount of fibrils formed in TBS buffer control samples that contained no metals was approximately a factor of seven lower than in PBS. The time for completion of the reactions increased about sixfold in TBS compared to PBS at the same SEVI peptide concentration. Tris,

similarly to phosphate, can associate with divalent metals (Aslamkhan et al. 2002). In 20 mM HEPES–150 mM NaCl, pH 7.0, which is a Good buffer (Good et al. 1966), that should interact minimally with metals, the ThT fluorescence plateau was a factor of ten lower and reaction times were increased threefold (data not shown). These results are consistent with a recent report that SEVI fibrillization is markedly enhanced in anionic buffers like phosphate (Olsen et al. 2012). We thus used PBS buffer for SEVI fibrillization studies because it consistently gave the best results, and because this buffer most closely replicates physiological conditions (Owen and Katz 2005).

In addition to SEVI peptide and buffer, each fibrillization reaction contained 15 μM amyloid-specific dye ThT to detect fibrils (LeVine 1993), 0.02 % (*v*/*v*) NaN_3 to prevent bacterial growth during the fibrillization reactions, and a Teflon bead which improves reproducibility by providing more efficient mixing of the reaction components (Giehm and Otzen 2010; Morris et al. 2009). The plates were maintained at 37 °C throughout the experiments. A continuous agitation speed of 240 rpm was used for the reactions. Although agitation is necessary for SEVI to form fibrils (Munch et al. 2007; Olsen et al. 2010) we found that increasing the agitation speed from 240 to 1,200 rpm had no effects on fibril formation kinetics. Fibrillization reactions were performed in triplicate to obtain estimates of the uncertainties of the kinetic data. The fluorescence of ThT was measured every 30 min on a Fluoroskan Ascent plate reader (Franklin, MA, USA) using excitation at 440 nm and emission at 490 nm (LeVine 1993). Lag times and rates of fibrillization reactions were obtained from nonlinear least-squares fits of the data to a published six-term equation (Cohlberg et al. 2002). Reaction plateaus were determined from the fluorescence maxima when the reactions first reached a steady-state. At longer times, once fibrils have formed, the solution is no longer homogeneous so that the fluorescence values can become unreliable (Volles and Lansbury 2007).

Transmission electron microscopy (TEM)

Samples for TEM were prepared from 1 mg/ml solutions of SEVI incubated, with continuous agitation, for 15 days in PBS buffer at pH 7.4 and 37 °C. The samples contained 1 mM $ZnCl_2$ or $CuCl_2$. We also investigated control samples without metals and containing 5 mM EDTA. ThT fluorescence was used to confirm that all fibrillization reactions had reached the plateau stage before imaging by TEM. Samples were applied to 400-mesh carbon-coated copper grids and negatively stained by use of 1 % uranyl acetate. The samples were applied to the grids in 4-μl volumes, then the grids were rinsed with 1 μl H_2O, and excess liquid was removed from the grid, by capillary action, by use of filter paper. To stain the samples, 4 μl 1 % uranyl acetate was applied for 45 s and the excess stain was removed with filter paper. Electron micrographs were obtained by use of an FEI Tecnai G^2 BioTWIN instrument, which is part of the UConn TEM facility.

Nuclear magnetic resonance (NMR) spectroscopy

NMR data were collected on a 600 MHz Varian Inova spectrometer equipped with a cryogenic probe. The experiments were preformed on 3 mM samples of SEVI in 90 % H_2O–10 % D_2O. The pH was adjusted to 5.5 or 7.4 by addition of 1 M HCl and NaOH solutions. The temperature for the experiments was 10 °C, to avoid loss of amide proton signals through solvent exchange. NMR assignments were obtained using 2D experiments from the Varian Protein Pack. Residue-type assignments were obtained from 70 ms mixing time TOCSY experiments and sequential assignments were from 300 ms mixing time NOESY spectra. These were supplemented with ^{1}H–^{15}N HSQC and C-α-selective ^{1}H–^{13}C HSQC spectra collected on samples at natural isotopic abundance to obtain ^{13}C and ^{15}N assignments. The acquisition conditions for these experiments are given in Supplementary Table S1. The NMR samples under quiescent conditions were stable at 10 °C as monitored by 1D NMR spectra collected before and after 2D NMR experiments. NMR assignments have been deposited in the BioMagResonBank (BMRB) under accession numbers 17924 (SEVI) and 17925 (SEVI with 4 mM $ZnCl_2$). To characterize line broadening in the presence of $ZnCl_2$ and $CuCl_2$, crosspeak volumes in ^{1}H–^{13}C HSQC and ^{1}H–^{15}N HSQC spectra were measured with the "integrator" utility of the iNMR software (Mestrelab Research).

Isothermal titration calorimetry (ITC)

Experiments were performed at 25 °C on a Nano ITC low-volume calorimeter (TA Instruments, New Castle, DE, USA). Samples were prepared in 20 mM Tris buffer at pH 7.5 containing 150 mM NaCl (TBS buffer). For the Cu^{2+} experiment, the SEVI concentration was 200 μM and the starting ligand concentration was 1 mM $CuCl_2$. Because of weaker binding, the experiment with Zn^{2+} required a SEVI concentration of 400 μM and a starting ligand concentration of 2 mM $ZnCl_2$. Because Zn^{2+} is poorly soluble at basic pH, the 2 mM $ZnCl_2$ solution in 20 mM TBS buffer was prepared by serial dilution, starting from a 200 mM $ZnCl_2$ stock solution prepared in de-ionized water. All solutions were filtered through 0.2 μm filters and degassed under vacuum for 15 min. Control titration experiments to obtain the heat of dilution were performed by titrating TBS solutions of 1 mM $CuCl_2$ or

2 mM $ZnCl_2$, against TBS buffer without protein. Control experiments showed that contributions from enthalpy changes as a result of dilution were negligible ($\Delta H < -1.0$ kJ/mol). ITC data were analyzed with NanoAnalyze software (v. 2.1.13).

Results

Cu^{2+} and Zn^{2+} inhibit SEVI fibrillization

Figure 1 shows the effects of increasing $CuCl_2$ (Fig. 1a) and $ZnCl_2$ (Fig. 1b) concentrations on SEVI fibrillization. Both metals inhibited fibrillization compared with control samples of SEVI containing 5 mM metal chelator EDTA. Additional controls experiments were used to establish that the presence of EDTA had no effect on the fibrillization kinetics of SEVI (not shown). The Zn^{2+} and Cu^{2+} ions are good ligands for histidines (Brender et al. 2010), which are present at positions 3 and 23 in the SEVI amino acid sequence. In addition to these metals, we also looked at the effects of 1 mM Ca^{2+} and Mg^{2+} which are poor ligands for histidine imidazole rings (Brender et al. 2010). Inhibition of fibrillization was observed with 1 mM $MgCl_2$ although to a lesser extent than with $CuCl_2$ or $ZnCl_2$. By contrast,

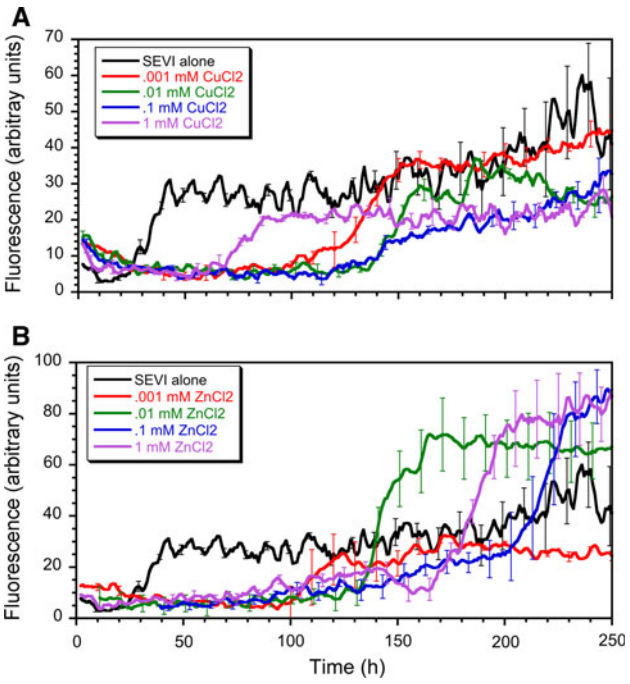

Fig. 1 Inhibition of SEVI fibrillization with increasing concentrations of **a** $CuCl_2$ and **b** $ZnCl_2$. All experiments were performed with 2 mg/ml SEVI in PBS buffer, pH 7.4, at 37 °C. *Error bars* are the standard errors of the mean values calculated from triplicate runs; for clarity they are shown every tenth point only

$CaCl_2$ had little effect compared with control samples without metals (Supplementary Fig. S2).

The fibrillization of SEVI follows nucleation kinetics typical of amyloid assembly (Sheftic et al. 2009). There is initially a lag time, because nucleation is entropically disfavored by loss of rotational and translational degrees of freedom when SEVI monomers aggregate. Once a critical mass or nucleus forms, the reaction enters a growth phase in which addition of monomers becomes enthalpically favorable as new non-covalent interactions form during the fibril elongation process. Eventually, the reaction reaches a steady state plateau in which ordered aggregates and monomers seem to be in equilibrium (Andreu and Timasheff 1986; Harper and Lansbury 1997). The effects of Zn^{2+} and Cu^{2+} on kinetic data characterizing SEVI fibrillization reactions—lag times, elongation rates, and plateaus—are shown in Fig. 2.

The most striking effect is on lag times for fibrillization (Fig. 2a). These increase four to eightfold in the presence of the metals compared with control samples containing SEVI alone, suggesting that the nucleation part of the reaction is inhibited in the presence of metals. A constant fourfold increase in lag times is observed for Cu^{2+} concentrations in the range between 0.001 and 0.1 mM, consistent with a low dissociation constant for Cu^{2+} (see the section "ITC shows SEVI forms oligomeric complexes with Cu^{2+} and Zn^{2+}", below). At the largest concentration of 1 mM $CuCl_2$, there is a reversion to shorter lag times but these nevertheless remain about two-fold longer than for SEVI without metals. The reason for the decrease in lag time at the highest 1 mM Cu^{2+} concentration compared with 0.1 mM Cu^{2+} is unclear but could indicate that under super-saturating concentrations of the metal additional binding sites become important. Lag times also increase with increasing Zn^{2+} concentrations, reaching a plateau at 0.1–1.0 mM $ZnCl_2$. These results are consistent with a Zn^{2+} dissociation constant in the range of $\sim$1 mM, a value approximately three orders of magnitude larger than that for Cu^{2+}.

At the lowest concentrations of Cu^{2+} and Zn^{2+} tested (0.001 mM), there is a two-fold reduction in fibril elongation rates compared with SEVI alone. This suggests that in addition to interfering with nucleation the metals hinder addition of SEVI monomers to the growing fibrils. As the metal concentration is increased to 1 mM, however, elongation rates decrease no further, within experimental uncertainty (Fig. 2b). The fluorescence plateaus, when the fibrillization reactions enter a steady state, decrease slightly with increasing Cu^{2+} concentrations, whereas they increase with increasing Zn^{2+} concentrations (Fig. 2c). In experiments performed with a lower SEVI peptide concentration, 1 mg/ml, the same increase in lag times and decrease in rates were observed but the fluorescence plateaus were

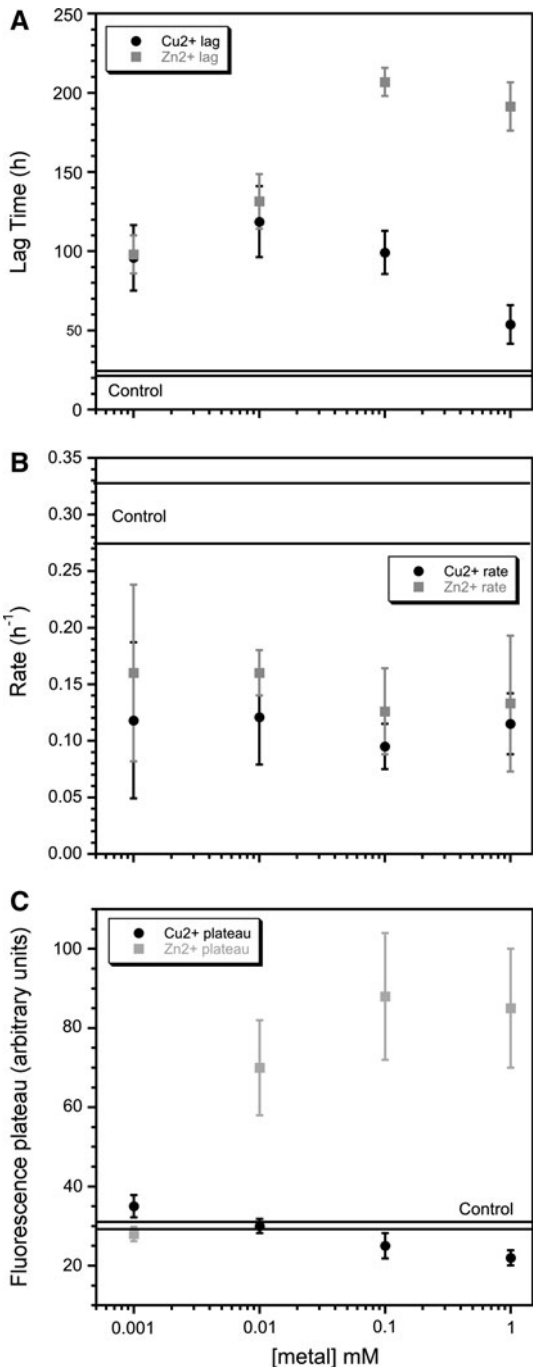

Fig. 2 Semi-logarithmic plots showing the $CuCl_2$ (*black*) and $ZnCl_2$ (*gray*) concentration dependence of kinetic data for SEVI fibrillization derived from the results depicted in Fig. 1. **a** Lag times. **b** Fibril growth rates. **c** ThT fluorescence plateaus. *Uncertainty bars* represent the standard errors in kinetic data from experiments run in triplicate. The *horizontal lines marked "control"* are ranges for results obtained from SEVI experiments without metals

reduced for both Cu^{2+} and Zn^{2+}. Fluorescence plateaus often correlate with the amount of fibrils formed but can also be affected by differences in fibril morphology that affect interactions with the dye ThT. Even if the larger fluorescence plateaus in the presence of 0.01–1.0 mM Zn^{2+} are because of a larger numbers of fibrils in the presence of large Zn^{2+} concentrations, the lag times under these conditions are increased eight to ninefold (Fig. 2a), so Zn^{2+} would be a potent inhibitor of fibrillization on physiological timescales.

In addition to experiments at pH 7.4, we also examined SEVI fibrillization under acidic pH conditions, when the two histidines in the protein are expected to be protonated and, thus, should have a poorer affinity for divalent metals. For these experiments we used 20 mM sodium acetate–150 mM NaCl buffer, pH 4.0 (Supplementary Fig. S3). $ZnCl_2$ concentrations over the range 0.001 to 1 mM had no apparent effects on fibrillization, within experimental uncertainty. Specifically, the differences between reactions at different $ZnCl_2$ concentrations were comparable with the variance between replicate experiments. In contrast with the results at physiological pH in PBS buffer when the two histidines in SEVI are uncharged, fibrillogenesis is no longer inhibited by $ZnCl_2$ at acidic pH when the two histidines are protonated.

Fibril morphology is unchanged but the amount of fibrils is reduced in the presence of Zn^{2+} and Cu^{2+}

Having established that Zn^{2+} and Cu^{2+} inhibit fibril formation, we next wanted to determine whether the metals affected the morphology of the fibrils. In Fig. 3, control SEVI fibrils formed in the absence of metals (Fig. 3a) are compared with fibrils formed in the presence of 1 mM $ZnCl_2$ (Fig. 3b) or $CuCl_2$ (Fig. 3c). High-magnification TEM images show that the metals have no apparent effects on fibril morphology. Lower-magnification images given in the insets for Fig. 3 suggest that the amount of SEVI fibrils is reduced in the presence of 1 mM $ZnCl_2$ or $CuCl_2$ compared with the control.

NMR mapping identifies the two histidines in SEVI as the ligands for Zn^{2+} and Cu^{2+}

We next used NMR to investigate the SEVI binding sites for Zn^{2+} and Cu^{2+}. Previous NMR studies revealed that the SEVI peptide is intrinsically unfolded at 37 °C but folds into an α-helical structure in 50 % trifluoroethanol similar to that of the corresponding 248–286 segment in the parent protein human prostatic acid phosphatase (Brender et al. 2011). In this work we conducted NMR experiments at 10 °C. Under these conditions, although the protein remains mostly unfolded, NOE connectivities and chemical shift deviations from random coil values are consistent with small amounts of residual α-helix structure populated at levels of ~25 to 35 % (Supplementary Fig. S4). The sequence pattern of secondary shifts and NOEs in water at

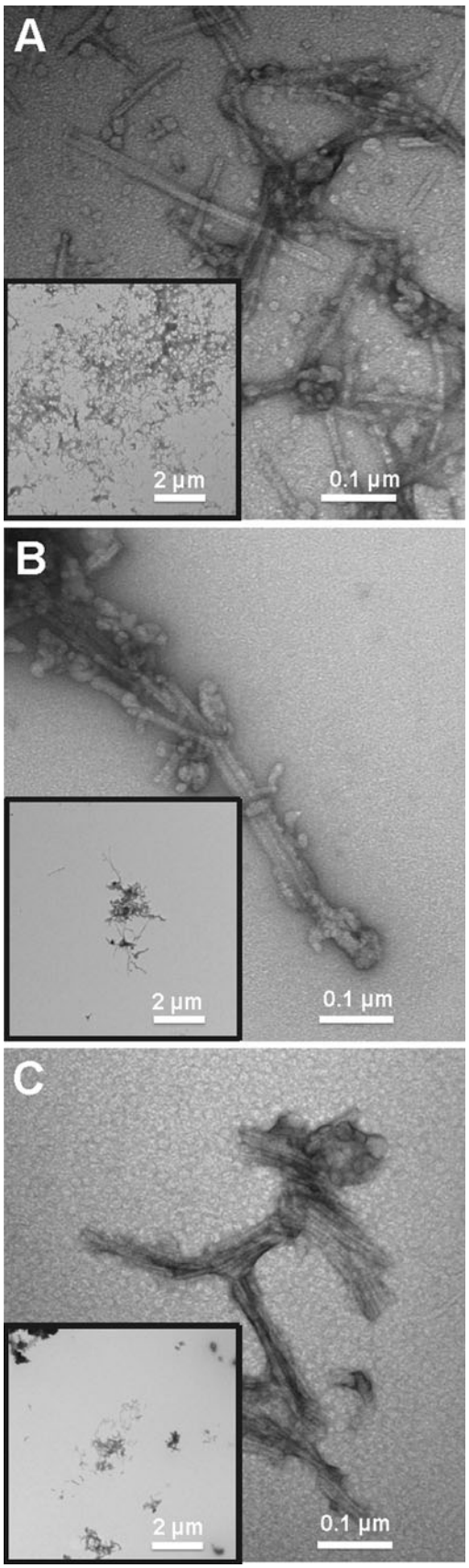

◀ **Fig. 3** TEM images of SEVI fibrils at ×150,000 magnification. SEVI fibrils were grown in the absence of metals (**a**; control experiment), in the presence of 1 mM $ZnCl_2$ (**b**), and in the presence of 1 mM $CuCl_2$ (**c**). The *insets* for each panel show images obtained at a lower magnification of ×11,000 to illustrate the decrease in the amount of fibrils formed when metals are present. Fibrils for TEM were prepared from 1 mg/ml solutions of SEVI in PBS buffer, pH 7.4, at 37 °C. ThT fluorescence was used to confirm that all fibrillization reactions had reached a steady-state plateau before imaging by TEM

10 °C (Supplementary Fig. S4b) is similar to that observed in 50 % trifluoroethanol at 37 °C, where the peptide adopts a native-like α-helical structure (Brender et al. 2011). Stabilization of the residual α-helix structure probably occurs because of the low temperature used for our NMR studies, as has been seen for other disordered peptides (Alexandrescu and Kammerer 2003; Steinmetz et al. 2007). NOE correlations for 2D ^{1}H NOESY spectra of SEVI in the presence of $ZnCl_2$ are little or no different from those for the free peptide, except that crosspeaks from residues near the two histidines are lost because of line broadening. We also compared Hα and Cα secondary chemical shifts of free and zinc-bound peptide and found only small differences, suggesting an increase of, at most, 5–10 % α-helical structure in the vicinity of histidines 3 and 23 when Zn^{2+} is bound (Supplementary Fig. S4c).

The changes in the NMR spectrum accompanying binding of diamagnetic zinc to SEVI are manifested as line-broadening, caused by intermediate exchange between the free and bound forms of the peptide. To better characterize the binding site, we collected 2D ^{1}H–^{15}N HSQC spectra of a 3 mM SEVI sample at natural isotopic abundance. Spectra were recorded in the absence of metals, in the presence of a 2:1 peptide-to-Zn^{2+} ratio, and at a 1:1.3 peptide-to-Zn^{2+} ratio (Fig. 4a). Losses in ^{1}H–^{15}N HSQC crosspeak volumes as a result of intermediate exchange between the free and bound peptide are localized to residues 2–6 and 23–24, flanking the two histidines at positions 3 and 23. Line broadening is observed at substoichiometric concentrations of Zn^{2+}, and additional decreases of crosspeak volumes are only small as the metal concentration becomes saturating. The magnitude of the line broadening effects is similar for the regions surrounding His3 and His23, suggesting the two histidines bind Zn^{2+} simultaneously (Fig. 4b). Consistent results implicating His3 and His23 as the ligands for Zn^{2+} were seen in ^{1}H–^{13}C HSQC spectra of SEVI, except that fewer residues could be analyzed because of the poorer chemical shift dispersion in the carbon spectrum (Supplementary Fig. S5).

We obtained analogous results for the binding of paramagnetic Cu^{2+} to SEVI except that a larger number of crosspeaks were broadened in the ^{1}H–^{15}N HSQC (Supplementary Fig. S6) and ^{1}H–^{13}C HSQC spectra (Supplementary Fig. S7). Although the sequence profiles are less

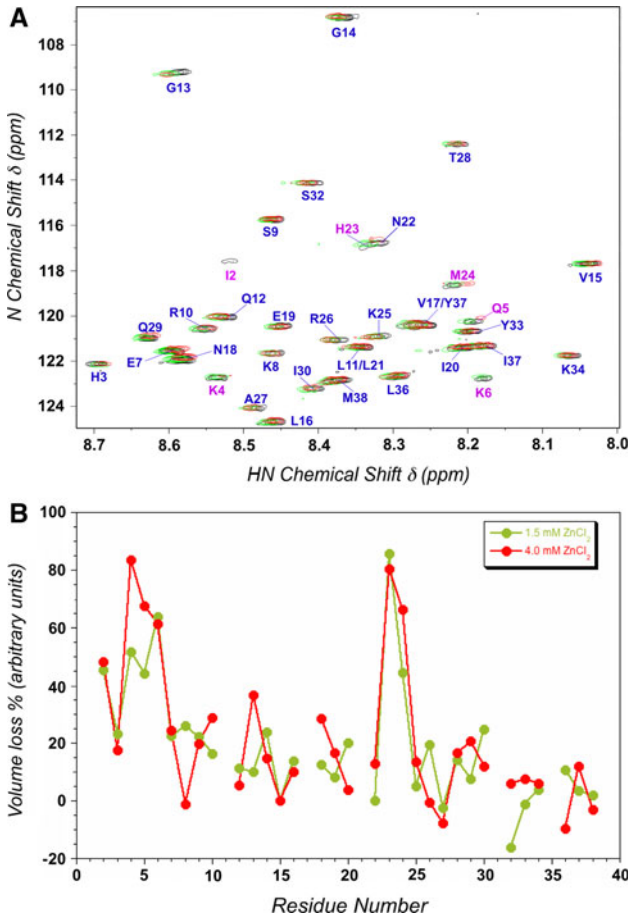

Fig. 4 Effects of $ZnCl_2$ on the NMR spectrum of SEVI. **a** The three superposed $^{1}H–^{15}N$ HSQC spectra were acquired on a 3 mM SEVI sample at natural ^{15}N abundance. The spectrum in the absence of zinc is shown in *black contours*, with 1.5 mM $ZnCl_2$ in *green*, and with 4 mM $ZnCl_2$ in *red*. Sequence-specific NMR assignments for SEVI are indicated with *blue text* for peaks that are unaffected and *purple text* for residues for which NMR signal broadening is observed in the presence of zinc. **b** Plot of crosspeak volume loss (%) with $ZnCl_2$, as a function of residue position in the SEVI sequence. The uncertainties in the volume loss values, estimated from the RMSD baseline noise of the spectra, are ~15 %

well-defined than with Zn^{2+}, the NMR results show that His3 and His23 also serve as the ligands for Cu^{2+}.

The NMR experiments described above were performed at pH 5.5 to minimize loss of amide proton peak intensities because of exchange with solvent. Indeed, most of the amide proton correlations in the $^{1}H–^{15}N$ HSQC spectrum of SEVI are lost on going from pH 5.5–7.4 (Supplementary Fig. S8). The hydrogen exchange half-times predicted for the highly cationic SEVI amino acid sequence by SPHERE software (Bai et al. 1993; Zhang 1995) at pH 7.4 and 10 °C are of the order of ~0.05 s. The half-times for exchange of the peptide approach the 10 ms delay constituting the four 1/4 J INEPT refocusing periods in the $^{1}H–^{15}N$ HSQC experiment, and are thus consistent with the observed loss of peaks going from pH 5.5–7.4. The pH of 5.5 used to minimize amide proton exchange, is approximately 1 pH unit lower than the typical pK_a of 6.5 for histidine. Under these conditions the two histidines in SEVI are likely to exist primarily in their protonated state, which could reduce their affinity for metals and interfere with mapping of the binding site by NMR. We consequently characterized binding of $CuCl_2$ (Supplementary Fig. S9) and $ZnCl_2$ (Supplementary Fig. S10) to SEVI at pH 7.4 by using $^{1}H–^{13}C$ HSQC experiments, because carbon-bound protons are not labile to exchange. The same sequence pattern of NMR line broadening effects observed at the acidic pH of 5.5 was observed at pH 7.4, indicating that histidines 3 and 23 are the ligands for Cu^{2+} and Zn^{2+} in SEVI under physiological conditions.

ITC shows SEVI forms oligomeric complexes with Cu^{2+} and Zn^{2+}

We next conducted ITC experiments to obtain information about the stoichiometry and thermodynamics of metal binding (Fig. 5). The titration for Cu^{2+} is well-defined and indicates that the metal binds with a substoichiometric Cu^{2+}-to-SEVI ratio of $n = 0.3$ and a dissociation constant of 2 μM (Fig. 5a). The value of $n = 0.3$ suggest SEVI binds Cu^{2+} as a trimer, in which His3 and His23 from three SEVI monomers constitute the ligands of an octahedral metal coordination site.

The ITC results indicate SEVI binds Zn^{2+} more weakly than Cu^{2+}, by a factor of three orders of magnitude. We obtained an apparent dissociation constant of 1.7 ± 0.9 mM, however, this value is subject to much uncertainty because of the weak affinity of SEVI for Zn^{2+}. Similarly, the *n*-value of 0.45 ± 0.40 obtained from ITC indicates substoichiometric binding but does not enable us to establish precisely how many SEVI molecules are bound to a Zn^{2+} ion. Whereas Cu^{2+} prefers octahedral or planar coordination in proteins (Creighton 1993), tetrahedral coordination is preferred for Zn^{2+} and octahedral coordination is rare (Silvennoinen et al. 2009).

Discussion

In this work we have shown that Zn^{2+} and Cu^{2+} inhibit SEVI fibril formation (Figs. 1, 2) but do not affect fibril morphology (Fig. 3). Inhibition is achieved by coordinating the two histidines at positions 3 and 23 in the SEVI sequence (Fig. 4) and is relieved when the histidines become protonated at acidic pH. Cu^{2+} is more effective at inhibiting SEVI fibrillization than Zn^{2+} and this correlates with the tighter binding of the former metal ion to SEVI (Fig. 5).

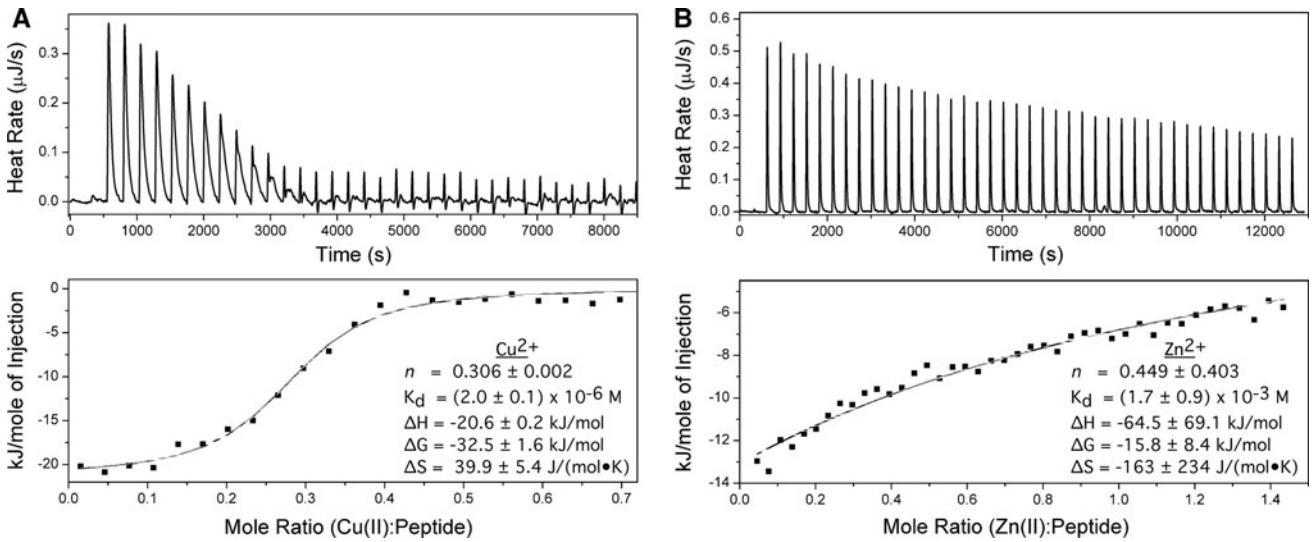

Fig. 5 ITC experiments measuring Cu^{2+} (**a**) and Zn^{2+} (**b**) binding to SEVI. The *upper panels* show the heat evolved during the titrations. The *lower panels* show the enthalpy changes with increasing metal-to-SEVI mole fraction. The data were fit to a single binding site (independent binding) model

The normal concentration of Cu^{2+} in human semen is 1–3 μM (Camejo et al. 2011; Huang et al. 2000), comparable with the K_d of 2 μM determined for binding of the metal to SEVI by ITC (Fig. 5a). Zinc concentrations in seminal plasma are approximately 2.5 mM (0.16 g/L) (Camejo et al. 2011; Huang et al. 2000; Owen and Katz 2005), higher than in any other body fluids or tissues (Bedwal and Bahuguna 1994; Huang et al. 2000). Although Zn^{2+} has a large K_d of 2 mM (Fig. 5b), the concentration of zinc in semen should be sufficiently high to bind SEVI under physiological conditions. Inhibition of SEVI fibrillization by metals could be relieved when the peptide is transferred to a different environment after intercourse. It has previously been shown that the ability of SEVI to enhance HIV infectivity is retained in the acidic environment of the vaginal tract (Munch et al. 2007). In the vaginal tract, concentrations of Cu^{2+} and Zn^{2+} are smaller than in semen (Bohler et al. 1994; Hagenfeldt 1972) and the acidic pH of 4.2 (Munch et al. 2007) would reduce affinity for these metals because of protonation of the histidine ligands. Another factor worth noting is that although our results suggest that Zn^{2+} inhibits SEVI fibrillization, the metal also restricts the activity of seminal proteases, for example prostate specific antigen (PSA), which may be involved in the degradation of SEVI fibrils (Olsen et al. 2012).

Cu^{2+} and/or Zn^{2+} have been reported to inhibit the fibrillization of several amyloidogenic peptides and proteins including amylin (Brender et al. 2010; Salamekh et al. 2011), insulin (Noormagi et al. 2010), Ab (Raman et al. 2005), and prion protein (Singh et al. 2010). A common theme that emerges from these studies is that the metals inhibit fibrillization by coordinating disordered segments of the polypeptide chains and inducing oligomeric structures that are not competent for fibril assembly. For amyloidogenic precursors that exist as folded globular proteins, for example transthyretin, a possible strategy to inhibit fibrillization is to develop molecules that bind, and thereby stabilize, the native state (Sacchettini and Kelly 2002). This work and previous work on the inhibition of amyloidogenic proteins by metals (Brender et al. 2010; Noormagi et al. 2010; Salamekh et al. 2011; Singh et al. 2010) suggests that compounds that bind and stabilize non-native structures incompatible with fibril assembly may lead to the development of inhibitors of amyloidogenic polypeptides that are intrinsically unfolded.

Conclusions

This investigation has provided new information about amyloid formation by the peptide SEVI, and its inhibition by metal ions. The effects of Cu^{2+} and Zn^{2+} are primarily to delay the formation of nuclei needed for SEVI fibril assembly. Although fibrillization is inhibited, the apparent morphology of fibrils formed in the presence or absence of metals is conserved at the resolution of electron microscopy. By using NMR spectroscopy we were able to map the metal binding sites to the two histidines in SEVI. Isothermal titration calorimetry indicates that Cu^{2+} binds SEVI with a micromolar dissociation constant while Zn^{2+} binds with a millimolar dissociation constant, and that SEVI forms oligomeric complexes with both metals. Although the K_d values for Cu^{2+} and Zn^{2+} are comparable

with the concentrations of these metals in human seminal plasma, the action of the SEVI in HIV infectivity is likely to be complex. Human semen contains a diverse mixture of compounds that could affect SEVI fibrillization, in addition to the metals considered in this work. Metals could have indirect effects on fibrillization, for example inhibiting proteases that degrade SEVI. Finally, the inhibitory effects of metals on SEVI fibrillization may be relieved when the peptide is transferred from semen to other body fluids. Our work could lead to more detailed understanding of the environmental factors that affect SEVI fibrillogenesis, information that could aid in the development of therapy to block the peptide's function in viral infectivity.

Acknowledgments We thank Molly Siegel and Tyler Daman for technical assistance during the early stages of this project and Dr Olga Vinogradova for use of her ITC machine. This work was supported by an NSF Graduate Research Fellowship to SRS, a UConn Summer Undergraduate Research Fellowship to JS, and by an American Diabetes Association Basic Science Award to ATA.

References

Alexandrescu AT, Kammerer RA (2003) Structure and disorder in the ribonuclease S-peptide probed by NMR residual dipolar couplings. Protein Sci 12:2132–2140

Andreu JM, Timasheff SN (1986) The measurement of cooperative protein self-assembly by turbidity and other techniques. Methods Enzymol 130:47–59

Aslamkhan AG, Aslamkhan A, Ahearn GA (2002) Preparation of metal ion buffers for biological experimentation: a methods approach with emphasis on iron and zinc. J Exp Zool 292:507–522

Bai Y, Milne JS, Mayne L, Englander SW (1993) Primary structure effects on peptide group hydrogen exchange. Proteins 17:75–86

Bedwal RS, Bahuguna A (1994) Zinc, copper and selenium in reproduction. Experientia 50:626–640

Bohler K, Meisinger V, Klade H, Reinthaller A (1994) Zinc levels of serum and cervicovaginal secretion in recurrent vulvovaginal candidiasis. Genitourin Med 70:308–310

Brender JR, Hartman K, Nanga RP, Popovych N, de la Salud Bea R, Vivekanandan S, Marsh EN, Ramamoorthy A (2010) Role of zinc in human islet amyloid polypeptide aggregation. J Am Chem Soc 132:8973–8983

Brender JR, Nanga RP, Popovych N, Soong R, Macdonald PM, Ramamoorthy A (2011) The amyloidogenic SEVI precursor, PAP248-286, is highly unfolded in solution despite an underlying helical tendency. Biochim Biophys Acta 1808:1161–1169

Camejo MI, Abdala L, Vivas-Acevedo G, Lozano-Hernandez R, Angeli-Greaves M, Greaves ED (2011) Selenium, Copper and Zinc in seminal plasma of men with varicocele, relationship with seminal parameters. Biol Trace Elem Res 143:1247–1254. doi: 10.1007/s12011-011-8957-5

Cohlberg JA, Li J, Uversky VN, Fink AL (2002) Heparin and other glycosaminoglycans stimulate the formation of amyloid fibrils from alpha-synuclein in vitro. Biochemistry 41:1502–1511

Collier HB (1979) Binding of Zn^{2+} by buffers. Clin Chem 25:495–496

Creighton TE (1993) Proteins: structures and molecular properties, 2nd edn. W. H. Freeman and Company, New York

Easterhoff D, DiMaio JT, Doran TM, Dewhurst S, Nilsson BL (2011) Enhancement of HIV-1 infectivity by simple, self-assembling modular peptides. Biophys J 100:1325–1334

Giehm L, Otzen DE (2010) Strategies to increase the reproducibility of protein fibrillization in plate reader assays. Anal Biochem 400:270–281

Good NE, Winget GD, Winter W, Connolly TN, Izawa S, Singh RM (1966) Hydrogen ion buffers for biological research. Biochemistry 5:467–477

Hagenfeldt K (1972) Intrauterine contraception with the copper-T device. 4. Influence on protein and copper concentrations and enzyme activities in uterine washings. Contraception 6:219–230

Harper JD, Lansbury PT Jr (1997) Models of amyloid seeding in Alzheimer's disease and scrapie: mechanistic truths and physiological consequences of the time-dependent solubility of amyloid proteins. Annu Rev Biochem 66:385–407

Hauber I, Hohenberg H, Holstermann B, Hunstein W, Hauber J (2009) The main green tea polyphenol epigallocatechin-3-gallate counteracts semen-mediated enhancement of HIV infection. Proc Natl Acad Sci USA 106:9033–9038

Hong S, Klein EA, Das Gupta J, Hanke K, Weight CJ, Nguyen C, Gaughan C, Kim KA, Bannert N, Kirchhoff F, Munch J, Silverman RH (2009) Fibrils of prostatic acid phosphatase fragments boost infections with XMRV (xenotropic murine leukemia virus-related virus), a human retrovirus associated with prostate cancer. J Virol 83:6995–7003

Huang YL, Tseng WC, Cheng SY, Lin TH (2000) Trace elements and lipid peroxidation in human seminal plasma. Biol Trace Elem Res 76:207–215

Kim KA, Yolamanova M, Zirafi O, Roan NR, Staendker L, Forssmann WG, Burgener A, Dejucq-Rainsford N, Hahn BH, Shaw GM, Greene WC, Kirchhoff F, Munch J (2010) Semen-mediated enhancement of HIV infection is donor-dependent and correlates with the levels of SEVI. Retrovirology 7:55

LeVine H 3rd (1993) Thioflavine T interaction with synthetic Alzheimer's disease beta-amyloid peptides: detection of amyloid aggregation in solution. Protein Sci 2:404–410

Martellini JA, Cole AL, Svoboda P, Stuchlik O, Chen LM, Chai KX, Gangrade BK, Sorensen OE, Pohl J, Cole AM (2011) HIV-1 enhancing effect of prostatic acid phosphatase peptides is reduced in human seminal plasma. PLoS ONE 6:e16285

Morgan CJ, Gelfand M, Atreya C, Miranker AD (2001) Kidney dialysis-associated amyloidosis: a molecular role for copper in fiber formation. J Mol Biol 309:339–345

Morris AM, Watzky MA, Finke RG (2009) Protein aggregation kinetics, mechanism, and curve-fitting: a review of the literature. Biochim Biophys Acta 1794:375–397

Munch J, Rucker E, Standker L, Adermann K, Goffinet C, Schindler M, Wildum S, Chinnadurai R, Rajan D, Specht A, Gimenez-Gallego G, Sanchez PC, Fowler DM, Koulov A, Kelly JW, Mothes W, Grivel JC, Margolis L, Keppler OT, Forssmann WG, Kirchhoff F (2007) Semen-derived amyloid fibrils drastically enhance HIV infection. Cell 131:1059–1071

Noormagi A, Gavrilova J, Smirnova J, Tougu V, Palumaa P (2010) Zn(II) ions co-secreted with insulin suppress inherent amyloidogenic properties of monomeric insulin. Biochem J 430:511–518

Olsen JS, Brown C, Capule CC, Rubinshtein M, Doran TM, Srivastava RK, Feng C, Nilsson BL, Yang J, Dewhurst S (2010) Amyloid-binding small molecules efficiently block SEVI (semen-derived enhancer of virus infection)- and semen-mediated enhancement of HIV-1 infection. J Biol Chem 285:35488–35496

Olsen JS, Dimaio JT, Doran TM, Brown C, Nilsson BL, Dewhurst S (2012) Seminal plasma accelerates semen-derived enhancer of viral infection (SEVI) fibril formation by the prostatic acid

phosphatase (PAP248-286) peptide. J Biol Chem 287:11842–11849
Owen DH, Katz DF (2005) A review of the physical and chemical properties of human semen and the formulation of a semen simulant. J Androl 26:459–469
Raman B, Ban T, Yamaguchi K, Sakai M, Kawai T, Naiki H, Goto Y (2005) Metal ion-dependent effects of clioquinol on the fibril growth of an amyloid beta peptide. J Biol Chem 280:16157–16162
Roan NR, Munch J, Arhel N, Mothes W, Neidleman J, Kobayashi A, Smith-McCune K, Kirchhoff F, Greene WC (2009) The cationic properties of SEVI underlie its ability to enhance human immunodeficiency virus infection. J Virol 83:73–80
Sacchettini JC, Kelly JW (2002) Therapeutic strategies for human amyloid diseases. Nat Rev Drug Discov 1:267–275
Salamekh S, Brender JR, Hyung SJ, Nanga RP, Vivekanandan S, Ruotolo BT, Ramamoorthy A (2011) A two-site mechanism for the inhibition of IAPP amyloidogenesis by zinc. J Mol Biol 410:294–306
Santner A, Uversky VN (2010) Metalloproteomics and metal toxicology of alpha-synuclein. Metallomics 2:378–392
Sheftic SR, Croke RL, LaRochelle JR, Alexandrescu AT (2009) Electrostatic contributions to the stabilities of native proteins and amyloid complexes. Methods Enzymol 466:233–258
Silvennoinen L, Sandalova T, Schneider G (2009) The polyketide cyclase RemF from Streptomyces resistomycificus contains an unusual octahedral zinc binding site. FEBS Lett 583:2917–2921
Singh N, Das D, Singh A, Mohan ML (2010) Prion protein and metal interaction: physiological and pathological implications. Curr Issues Mol Biol 12:99–107
Steinmetz MO, Jelesarov I, Matousek WM, Honnappa S, Jahnke W, Missimer JH, Frank S, Alexandrescu AT, Kammerer RA (2007) Molecular basis of coiled-coil formation. Proc Natl Acad Sci USA 104:7062–7067
Tougu V, Tiiman A, Palumaa P (2011) Interactions of Zn(II) and Cu(II) ions with Alzheimer's amyloid-beta peptide. Metal ion binding, contribution to fibrillization and toxicity. Metallomics 3:250–261
Volles MJ, Lansbury PT Jr (2007) Relationships between the sequence of alpha-synuclein and its membrane affinity, fibrillization propensity, and yeast toxicity. J Mol Biol 366:1510–1522
Wurm M, Schambach A, Lindemann D, Hanenberg H, Standker L, Forssmann WG, Blasczyk R, Horn PA (2010) The influence of semen-derived enhancer of virus infection on the efficiency of retroviral gene transfer. J Gene Med 12:137–146
Zhang Y-Z (1995) Protein and peptide structure and interactions studied by hydrogen exchange and NMR. Ph.D. Thesis, University of Pennsylvania